Structural behavior of fluids from the vapor and liquid region to the supercritical phase

James Losey and Richard J. Sadus*
Centre for Computational Innovations, Swinburne University of Technology, PO Box 218, Hawthorn, VIC, 3122, Australia

(Received 3 June 2019; revised manuscript received 10 October 2019; published 22 November 2019)

A metric (χ) is introduced to quantify the relative proportion of particles having a specified number of near neighbors that are characteristic of liquid-phase properties. It can be used as a simple alternative to other methods for the investigation of some aspects of percolation behavior. Values of χ are obtained from molecular-dynamics simulations spanning the heterogeneous vapor and liquid region and the supercritical phase of the Lennard-Jones fluid. The supercritical phase can be delineated into regions of different structural properties. At different isochoric subcritical conditions, the temperature versus χ behavior shows evidence of inflections, which are associated with the onset of transitions from the vapor and liquid region to the supercritical phase. The analysis suggests a phenomenological requirement for the critical point in terms of a near-equal proportion of near neighbors with gaslike and liquidlike characteristics.

DOI: 10.1103/PhysRevE.100.052132

I. INTRODUCTION

The phase diagram of a pure fluid [1] delineates regions of both homogeneous and heterogeneous phases. At temperatures (T) below the triple point, vapor- and liquid phases coexist together. At higher T and densities (ρ), many fluids exhibit two-phase coexistence between solid and liquid phases that extend to high pressures (p), providing a demarcation between single liquid and solid phases. The unique characteristic of real fluids is the vapor-liquid critical point [2], which marks the termination of vapor-liquid equilibria (VLE) and the commencement of the supercritical phase.

The supercritical phase can exhibit some remarkable features [3]. For example, the supercritical phase of water [4] has enhanced solvating properties that are unexpected for the range of ρ and T. At moderate to high T [5–7], the isochoric (C_v) and isobaric heat capacities (C_p) display maximum values and there is evidence from theoretical studies [7–9] that both C_v and C_p may have minimum values. Over a narrow range of slightly supercritical T, the T-p coordinates of the maximum value of different thermodynamic functions merge onto a common curve, known as the Widom line [10,11]. The properties of the supercritical phase can be subdivided [11–13] based on dynamical properties, such as the speed of sound, resulting in the Frenkel line [14]. It is been proposed that fluids form clusters [15,16] at supercritical conditions, which may help explain some of its properties particularly in the context of percolation [17]. Diffraction studies for water [17,18] have defined a percolation threshold as the demarcation line between gaslike and liquidlike supercritical states.

Previous work [10–14,19–26] on the structural properties of the supercritical phase has largely focused on a narrow range of conditions that are typically close to either the Widom [10] or Frenkel [14] lines. Nishikawa *et al.* [19] observed supercritical density fluctuations in van der Waals fluids and small-angle neutron-scattering measurements [20] distinguished between gaslike and liquidlike properties in supercritical carbon dioxide. It has been reported [21] that the Widom line has a role in demarcating supercritical phenomena of different structure. Velocity autocorrelation function molecular-dynamics calculations [23] indicate hydrodynamic anomalies. Transitions between gaslike and solidlike structures have also been investigated [24,25] in the context of a Frenkel [14] line.

The aim of this work is to examine the transition from the vapor and liquid region to the supercritical state from the perspective of the change of the structural properties of the fluid. It is of interest to examine the changes of near neighbors between particles in the vapor, liquid, and supercritical states. Molecular-dynamics (MD) data for a near-neighbor metric are reported at state points spanning both the subcritical and supercritical regions. In contrast to previous studies [19–26], the nature of the transition between vapor and liquid is studied over a very wide range of conditions, covering both one-phase and two-phase subcritical regions and the supercritical phase.

II. METHODS

A. Molecular simulation details

MD microcanonical ensemble simulations [27] were performed for $N = 2000$ Lennard-Jones (LJ) particles [28] to obtain data for the number of near neighbors. The LJ potential [$u(r)$] is

$$u(r) = 4\varepsilon\left[\left(\frac{\sigma}{r}\right)^{12} - \left(\frac{\sigma}{r}\right)^{6}\right], \tag{1}$$

where r is the interparticle separation, ε is the minimum well depth, and σ is the distance at which $u(r) = 0$. The particles were initially placed on a face-centered-cubic lattice and the equations of motion were integrated using a five-value Gear predictor-corrector algorithm [27,29] with a reduced time step of 0.003. The cutoff distance was half of the box length

*rsadus@swin.edu.au

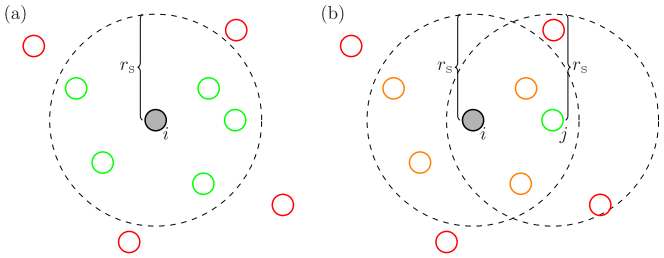

FIG. 1. Comparison of the (a) Stillinger and (b) TWF approaches for determining near neighbors. The colored circles represent particles at a given instance of time. In (a) the solid gray reference particle (i) has five neighbors inside the threshold distance of r_S and the four red particles (outside of the dashed circle) are not counted as neighbors. In (b), the i particle has the same five neighbors but only the green particle (j) has five neighbors within its own r_S radius, which now involves two of the red particles excluded in (a).

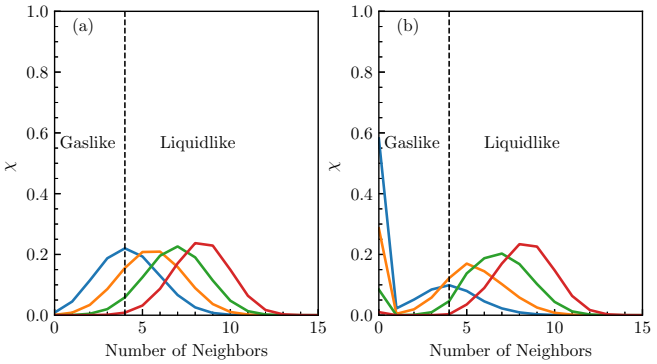

FIG. 2. Comparison of the fraction of $N = 2000$ LJ particles with respect to the number of near neighbors obtained from the (a) Stillinger and (b) TWF methods at $T = 1.65$ and from left to right $\rho = 0.3$ (blue line), 0.4 (orange line), 0.5 (green line), and 0.6 (red line). The vertical dashed line represents the division between gaslike ($\leqslant$4 neighbors) and liquidlike (>4 neighbors) properties.

and long-range corrections [27] were applied. The equilibration period was 5×10^5 time-steps and a further 1×10^6 time-steps were used to accumulate ensemble averages. The statistical uncertainties were close to the symbol size used to represent the data and error bars are omitted from the figures. The temperature ($T^* = kT/\varepsilon$, k is Boltzmann's constant) and density ($\rho^* = \rho\sigma^3$) are reported in dimensionless units and the asterisk superscript is hereafter omitted.

B. Near-neighbor counting algorithms

Studying the structure of heterogeneous fluids requires techniques that typically involve classifying properties based on the number of near neighbors [16,30]. We implemented two simple alternatives, namely the Stillinger [15] approach and its modification by ten Wolde and Frenkel (TWF) [31].

The Stillinger approach [Fig. 1(a)] defines a neighbor as any particle that is contained within a specified radial distance ($r_S = 1.5\sigma$), which is typically within the first coordination shell. This method is both simple and intuitive but some limitations have been documented for particle clusters. For example, at any given time step, a particle within the r_S threshold could have a high velocity relative to the reference particle, which would leave it outside of r_S at the next time step.

The TWF approach [see Fig. 1(b)] requires all neighbor particles to also have at least five neighbors within r_S. This additional requirement removes some of the overcounting of incidental surface particles. At high densities, the Stillinger and TWF counting approaches are expected to converge to the same values because the majority of the particles are located within 1.5σ. At low densities, the TWF approach could undercount neighbors by omitting small clusters and surface neighbors. The vapor phase typically has four or fewer neighbors, providing a convenient heuristic for identifying the characteristics of gaslike and liquidlike properties.

Rather than discussing the absolute number of particles with i near neighbors in the fluid, it is both more convenient and meaningful to report the fraction of particles (χ) that have $i > 4$ near neighbors, i.e., the fraction of particles with liquidlike characteristics

$$\chi = \frac{n_{i>4}}{N}. \tag{2}$$

In Eq. (2), $n_{i>4}$ is the total number of particles with liquidlike coordination. The values of χ range between 0 (no particles with liquidlike coordination) to 1 (all particles have liquidlike coordination). There is no unique definition of a nearest neighbor and using a value of 4 is a somewhat arbitrary value that is nonetheless commonly used.

Using a Voronoi construction [32] is a possible alternative, which is based on geometry and is parameter-free. However, it is both computationally expensive and prone to thermal fluctuations. These two disadvantages are overcome by the solid-angle-based nearest-neighbor (SANN) algorithm [33], which has its own unique definition of nearest neighbors. It is more computationally expensive than either the Stillinger or TWF approaches because it involves sorting all possible neighbors by distances and an iterative process starting with three minimum neighbors. Van Meel *et al.* [33] concluded that the SAAN algorithm yields results of similar reliability to cutoff-based approaches for the two-phase vapor-liquid equilibria of Lennard-Jones fluids. The simpler Stillinger and TWF approaches are appropriate for the calculation of χ.

III. RESULTS AND DISCUSSION

The differences in the distribution of χ values with respect to the number of near neighbors for the two methods were evaluated at different values of ρ in the supercritical phase (Fig. 2). The Stillinger method results in a bell-shape distribution, centered on the mean number of neighbors. The peak heights for the Stillinger method at different values of ρ are relatively uniform, whereas the TWF method generates a bimodal distribution with a peak for 0 neighbors that increases in height with decreasing ρ. The peak at 0 is a consequence of including particles that fall outside of the scope of the neighbor criterion such as particles associating in small clusters or on the surface of a cluster.

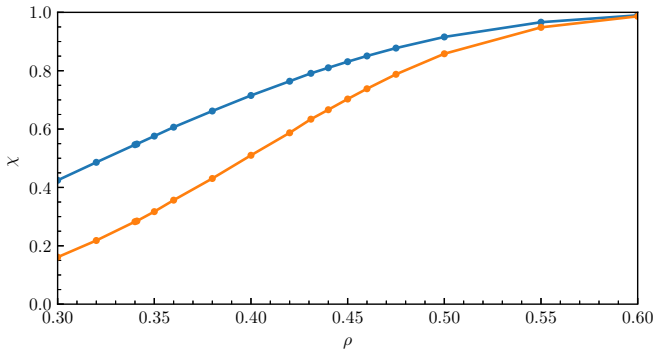

FIG. 3. Comparison of Stillinger (upper blue circles) and TWF (lower orange circles) χ values for 2000 LJ particles as a function of ρ for a liquidlike state (>4 near neighbors) at $T = 1.65$.

Figure 3 compares χ as a function of ρ in the supercritical phase at $T = 1.65$ for liquidlike states using the two methods. There is good agreement between the alternative procedures for $\rho > 0.55$, whereas the values of χ diverge considerably at lower ρ. At low ρ, the proportion of particles in the liquidlike state predicted by the TWF approach is considerably lower than that obtained for the Stillinger approach. The main differences between the alternative approaches are likely to become most apparent at low ρ.

Figure 4 compares T as a function of χ using either the (a) Stillinger or (b) TWF near-neighbor counting methods for ρ from 0.3 to 0.75, which are likely to have liquidlike character at some values of T. Figure 4 also includes the T-χ coordinates of the supercritical maximum (minimum) C_v and C_p data. The Stillinger and TWF approaches yield outcomes that are qualitatively identical. The main quantitative difference between the two approaches is that the Stillinger results

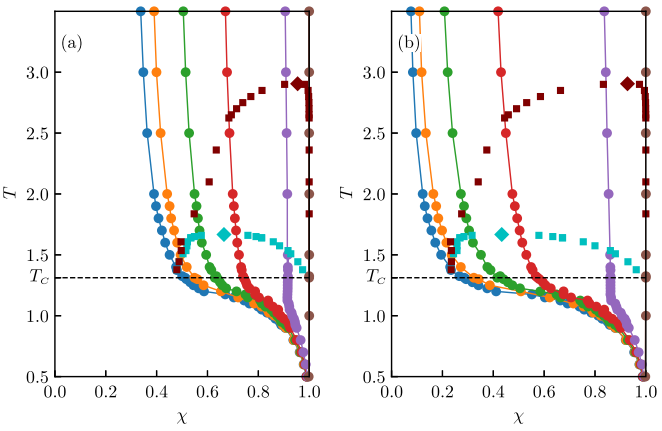

FIG. 4. The behavior of T with respect to χ at different isochores using the (a) Stillinger and (b) TWF methods. The different circles represent from left to right $\rho = 0.3$ (blue), 0.316 (orange), 0.35 (green), 0.4 (red), 0.5 (purple), and 0.75 (brown, very close to the $\chi = 1$ region) isochores. The horizontal dashed line represents $T_c = 1.312$ [34]. The squares are the supercritical maximum (minimum) values [8] of C_v (lower aquamarine squares) and C_p (upper brown squares), with the extremum for these properties given by the diamond of the same color.

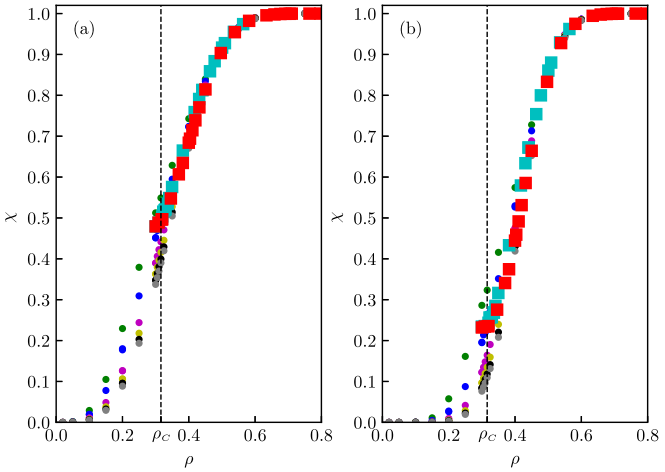

FIG. 5. χ-ρ behavior at critical ($T_c = 1.312$) and supercritical ($T > 1.312$) values of T the (a) Stillinger and (b) TWF methods. The different circles represent from left to right $T = 1.312$ (green), 1.5 (blue), 2.0 (purple), 2.5 (lime), 3.0 (black), and 3.5 (gray). The values corresponding to the minimum (maximum) [8] of both C_v (aquamarine squares) and C_p (red squares) are illustrated. The vertical dashed line represents $\rho_c = 0.316$.

[Fig. 4(a)] are restricted to a narrower range of values than the TWF [Fig. 4(b)] values. This is consistent with Fig. 3, which showed a larger spread of values across the range of liquid ρ.

At $\rho = 0.75$, the LJ fluid has liquid-density-like characteristics at all T, including in the two-phase liquid-vapor region; therefore, it is unsurprising that the T vs χ behavior is almost vertical [Figs. 5(a) and 5(b)]. The behavior at $\rho = 0.5$ is of interest because it spans both liquidlike and gaslike properties. Commencing at T values in the subcritical ($T < 1.312$) [34] vapor-liquid region, liquidlike values of χ decline before abruptly halting and thereafter falling within a narrow range up to high T.

For $\rho \leqslant 0.4$, the transition to lower χ values initially occurs much more gradually, passing through a region of near-constant gradient before rapidly turning upward to high T. The relative flatness of the T values close to the increase in gradient strongly suggests that the data may go through a point of inflection, i.e., $\partial T/\partial\chi = \partial^2 T/\partial\chi^2 = 0$ and $\partial^3 T/\partial\chi^3 \neq 0$. In effect, it is a structural analog of the point of inflection that characterizes the pressure-volume relationship of a pure fluid along the critical isotherm. It is impossible to reliably evaluate these criteria from the simulations and the evidence for inflection is entirely phenomenological. Therefore, although we will denote this phenomenon as an inflection, it is important to be mindful of the above caveats.

The inflection-point χ value decreases with decreasing values of ρ. For all values of ρ, the corresponding transition towards the inflection T commences over range of values below the VLE coexistence curve. The data are not sufficiently precise to accurately assign exact numerical values for the ρ, χ, or T at the inflection points. The inflection T probably occurs either at or slightly above the spinodal curve that separates metastable and nonstable regions of vapor and liquid coexistence. For the critical isochore ($\rho_c = 0.316$) [34], the inflection probably occurs at $T_c = 1.316$ because

both the spinodal and VLE curves meet at the critical point. It is important not to overemphasize the implications for real fluid behavior because the LJ potential is an approximate model that will deviate from the properties of real fluids and the near-critical region is particularly problematic [29,35–37].

The supercritical phase of the LJ fluid [8] exhibits both maximum and minimum values of C_v and C_p. These data appear to obey the laws applying to critical exponents, merging at distinct extremum points (ρ_E, T_E). We analyzed these data to determine the corresponding T-χ behavior. That is, for each reported T and ρ values, simulations were performed to determine the corresponding χ (see Fig. 4) from both the Stillinger and TWF methods. It is apparent that the isochores intersect both the C_v and C_p data. The points of intersection occur on both the C_v maximum and C_v minimum parts of the curves, i.e., at χ values both below and above that of the extremum point (χ_E). This indicates that the supercritical minimum in C_v is the result of liquidlike properties (high χ values) whereas the corresponding maximum values are associated with gaslike properties (low χ values). In contrast, the intersections with the C_p data occur exclusively before χ_E, i.e., on the maximum C_p part of the curve. Therefore, maximum C_p values occur for a wide range of fluid properties, whereas the C_p minimum is confined to a narrow range of liquidlike behavior.

The χ-ρ behavior at different constant values of T for the (a) Stillinger and (b) TWF approaches is illustrated in Fig. 5. The two approaches yield qualitatively similar results with the Stillinger χ values decaying to 0 slightly more slowly than the TWF values. This means that at $T_c = 1.312$, $\rho_c = 0.316$, $\chi_c \approx 0.5$ or 0.3 for the Stillinger and TWF approaches, respectively. The Stillinger analysis provides the convenient phenomenological insight that the vapor-liquid critical transition occurs when close to half of the LJ particles have liquidlike coordination. In view of the bimodal distribution observed [Fig. 2(b)] for the TWF, it is likely that the results for the Stillinger method more accurately reflect the true situation.

Another insight from either Figs. 5(a) or 5(b) is that for any given value of ρ the $T_c = 1.312$ isotherm yields the maximum value of χ. The comparison also includes the corresponding χ and ρ values for the supercritical maximum (minimum) of C_p and C_v. These values closely coincide with values obtained from the critical isotherm, particularly for the Stillinger analysis [Fig. 5(a)].

We observe that some of the general features of the behavior in Fig. 5 are superficially similar to aspects of percolation fraction behavior [37]. Percolation phenomena and structural properties are certainly related, which is apparent from theoretical work [39] involving squares and cubes. Other workers [37–39] have discussed the concept of percolation as a useful framework for identifying like-like clustering. In this context, the $\chi > 4$ criterion developed here could arguably be equivalent to whether or not a site is occupied. As such, it could also prove useful in identifying the percolation threshold in a much more computationally efficient way than alternative models. Unlike previous approaches, it is apparent that χ both extends in to the subcritical region and undergoes an inflection prior to reaching the critical temperature (see Fig. 4).

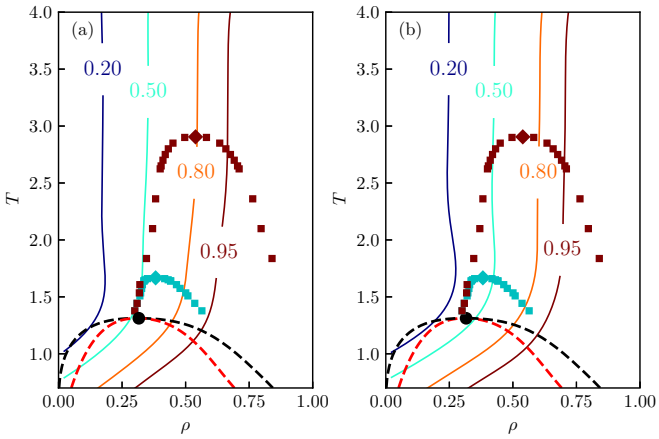

FIG. 6. T-ρ behavior of the LJ fluid at constant values of χ obtained for the (a) Stillinger and (b) TWF methods. Results are illustrated from left to right for $\chi = 0.2$ (blue line), 0.5 (aquamarine line), 0.8 (orange line), and 0.95 (brown line). Also illustrated are VLE (upper black dashed line) and spinodal (lower dashed red line) boundaries calculated from the Johnson *et al.* [40] equation of state; the critical point (black circle); and the supercritical maximum (minimum) values [8] of C_v (lower aquamarine squares) and C_p (upper brown squares), with the extremum for these properties given by the diamond of the same color.

The simulation data can be transformed to a conventional T-ρ projection (Fig. 6). The values of constant χ lines were obtained by interpolating between simulated state points using a radial basis function [41] that calculates a weighted sum from N data points based on a distance metric. In Fig. 6, lines of constant χ are overlaid on both the VLE and spinodal curves calculated for the Johnson *et al.* [40] LJ equation of state using the techniques described elsewhere [42–44].

The behaviors of the Stillinger and TWF constant χ lines are qualitatively similar in the supercritical region; the χ lines are broadly straight and parallel to each other. In all cases, the lines turn noticeably to lower ρ as the VLE line is approached, continuing to much lower ρ values in the vapor-liquid region. The $\chi = 0.5$ line approximately passes through ρ_c, which is also consistent with the analysis illustrated in Figs. 4 and 5.

IV. CONCLUSIONS

The near-neighbor fraction, χ, provides a useful metric for quantifying the structural characteristics of fluids that can be applied without any conceptual difficulty to both homogeneous and heterogeneous regions. It is also a computationally efficient method for the investigation of some features of percolation phenomena.

The MD data provide evidence of an inflection in T with respect to χ near the onset of the transition from two-phase vapor and liquid coexistence to supercritical behavior. This provides an insight into the role of cohesion, as represented by changes of near neighbors, on this important transition. For most values of ρ, the inflection T for the LJ fluid probably occurs either at or in the near vicinity of the T for the spinodal curve. For the critical isochore, the inflection point occurs at T_c.

The analysis of χ data provides a possible phenomenological requirement for the critical point of the LJ fluid. That is, the critical point requires that half of the particles have gaslike properties generally resulting in four or fewer neighbors.

Extending the calculation of χ into the supercritical phase clearly delineates regions of gaslike and liquidlike behavior. Comparison with MD data for the maximum (minimum) for C_v and C_p in the supercritical phase indicates that the maximum values for C_v are associated with gaslike near neighbors, whereas the minimum values coincide with liquidlike neighbors. In contrast, C_p maximum values are associated with a wide range of fluid properties with supercritical C_p minimum values confined to a narrow range of highly liquidlike behavior.

ACKNOWLEDGMENTS

J.L. thanks Swinburne University of Technology for a postgraduate research stipend. The simulations were performed using the Swinburne University of Technology supercomputer (OzSTAR).

[1] R. J. Sadus, *High Pressure Phase Behaviour of Multicomponent Fluid Mixtures* (Elsevier, Amsterdam, 1992).
[2] R. J. Sadus, AIChE J. **40**, 1376 (1994).
[3] *Supercritical Fluids: Fundamentals for Application*, edited by E. Kiran and J. H. M. Levett Sengers, NATO ASI Series Vol. 273 (Springer, Dordrecht, 1994).
[4] E. U. Franck, J. Chem. Thermodyn. **19**, 225 (1987).
[5] *Heat Capacities: Liquids, Solutions and Vapours*, edited by E. Wilhelm and T. Letcher (RSC Publishing, Cambridge, 2010).
[6] A. I. Abdulagatov, G. V. Stepanov, I. M. Abdulagatov, A. E. Ramaznova, and G. S. Alidultanova, Chem. Eng. Commun. **190**, 1499 (2003).
[7] N. G. Polikhronidi, I. M. Abdulagotov, R. G. Butyrova, G. V. Stepanov, J. T. Wu, and E. E. Ustuzhanin, Int. J. Thermophys. **33**, 185 (2012).
[8] T. M. Yigzawe and R. J. Sadus, J. Chem. Phys. **138**, 194502 (2013).
[9] J. Mairhofer and R. J. Sadus, J. Chem. Phys. **139**, 154503 (2013).
[10] L. Xu, P. Kumar, S. V. Buldyrev, S.-H. Chen, P. H. Poole, F. Sciortino, and H. E. Stanley, Proc. Natl. Acad. Sci. USA **102**, 16558 (2005).
[11] V. V. Brazhkin, Y. D. Fomin, A. G. Lyapin, V. N. Ryzhov, and E. N. Tsiok, J. Chem. Phys. B **115**, 14112 (2011).
[12] D. Bolmatov, V. V. Brazhkin, Y. D. Fomin, V. N. Ryzhov, and K. Trachenko, J. Chem. Phys. **139**, 234501 (2013).
[13] D. Bolmatov, V. V. Brazhkin, and K. Trachenko, Nat. Commun. **4**, 2331 (2013).
[14] V. V. Brazhkin, Y. D. Fomin, A. G. Lyapin, V. N. Ryzhov, E. N. Tsiok, and K. Trachenko, Phys. Rev. Lett. **111**, 145901 (2013).
[15] F. H. Stillinger, Jr., J. Chem. Phys. **38**, 1486 (1963).
[16] J. Wedekind and D. Reguera, J. Chem. Phys. **127**, 154516 (2007).
[17] M. Bernabei, A. Botti, F. Bruni, M. A. Ricci, and A. K. Soper, Phys. Rev. E **78**, 021505 (2008).
[18] M. Bernabei and M. A. Ricci, J. Phys.: Condens. Matter **20**, 494208 (2008).
[19] K. Nishikawa, K. Kusano, and A. A. Arai, J. Chem. Phys. **118**, 1341 (2003).
[20] T. Sato, M. Sugiyama, K. Itoh, K. Mori and T. Fukunaga, M. Misawa, T. Otomo, and S. Takata, Phys. Rev. E **78**, 051503 (2008).
[21] G. G. Simeoni, T. Bryk, F. A. Gorelli, M. Krisch, G. Ruocco, M. Santoro, and T. Scopigno, Nat. Phys. **6**, 503 (2010).
[22] J. Luo, L. Xu, E. Lascaris, H. E. Stanley, and S. V. Buldyrev, Phys. Rev. Lett. **112**, 135701 (2014).
[23] R. E. Ryltsev and N. M. Chchelkatchev, J. Chem. Phys. **141**, 124509 (2014).
[24] T. J. Yoon, M. Y. Ha, E. A. Lazar, W. B. Lee, and Y.-W. Lee, Phys. Chem. Lett. **9**, 6524 (2018).
[25] T. J. Yoon, M. Y. Ha, W. B. Lee, and Y.-W. Lee, Phys. Chem. Lett. **9**, 4550 (2018).
[26] T. J. Yoon, M. Y. Ha, W. B. Lee, and Y.-W. Lee, J. Chem. Phys. **149**, 014502 (2018).
[27] R. J. Sadus, *Molecular Simulation of Fluids: Theory, Algorithms and Object-Orientation* (Elsevier, Amsterdam, 1999).
[28] J. E. Jones, Proc. R. Soc. London, Ser. A **106**, 463 (1924).
[29] R. J. Sadus, Phys. Rev. E **99**, 012139 (2019).
[30] P. Senger, P. Schaaf, D. S. Corti, R. Bowles, J. C. Voegel, and H. Reiss, J. Chem. Phys. **110**, 6421 (1999).
[31] P. R. ten Wolde and D. Frenkel, J. Chem. Phys. **109**, 9901 (1998).
[32] A. Okabe, B. Boots, K. Sugihara, and S. N. Chiu, *Spatial Tessellations: Concepts and Applications of Voronoi Diagrams* (Wiley, New York, 2000).
[33] J. A. van Meel, L. Filion, C. Valeriani, and D. Frenkel, J. Chem. Phys. **136**, 234107 (2012).
[34] J. J. Potoff and A. Z. Panagiotopoulos, J. Chem. Phys. **109**, 10914 (1998).
[35] L. V. Woodcock, Int. J. Thermophys. **35**, 1770 (2014).
[36] J. V. Sengers and M. A. Anisimov, Int. J. Thermophys. **36**, 3001 (2015).
[37] D. M. Heyes and J. R. Melrose, Mol. Phys. **66**, 1057 (1989).
[38] D. R. Baker, G. Paul, S. Sreenivasan, and H. E. Stanley, Phys. Rev. E **66**, 046136 (2002).
[39] A. L. R. Bug, S. A. Safran, G. S. Grest, and I. Webman, Phys. Rev. B **33**, 4716 (1985).
[40] J. K. Johnson, J. A. Zollweg, and K. E. Gubbins, Mol. Phys. **78**, 591 (1993).
[41] W. H. Press, B. P. Flannery, S. A. Teukolsky, and W. T. Vetterling, *Numerical Recipes in C: The Art of Scientific Computing*, 3rd ed. (Cambridge University Press, Cambridge, 2007), pp. 139–143.
[42] R. J. Sadus, J. Chem. Phys. **115**, 1460 (2001).
[43] R. J. Sadus, J. Chem. Phys. **116**, 5913 (2002).
[44] R. J. Sadus, J. Phys. Chem. B **122**, 7757 (2018).